

Ram, S., Chao, J., Prabhat, P., Ward, E. S., and Ober, R. J. Overcoming the depth discrimination barrier in widefield microscopes: 3D single molecule tracking with high axial accuracy. In *Single Molecule Spectroscopy and Imaging. SPIE International Symposium on Biomedical and Optics (BiOs)*, 6862: 6862-00, 2008.

Copyright 2009 Society of Photo-Optical Instrumentation Engineers. One print or electronic copy may be made for personal use only. Systematic reproduction and distribution, duplication of any material in this paper for a fee or for commercial purposes or modification of the content of the paper are prohibited.

<http://dx.doi.org/10.1117/12.763097>

Overcoming the depth discrimination barrier in widefield microscopes: 3D single molecule tracking with high axial accuracy

Sripad Ram¹ and Jerry Chao^{1,2} and Prashant Prabhat^{1,2} and E. Sally Ward¹ and Raimund J. Ober^{1,2}

¹Department of Immunology, University of Texas Southwestern Medical Center, Dallas, TX, 75390, ²Department of Electrical Engineering, University of Texas at Dallas, Richardson, TX, 75083.

ABSTRACT

Current widefield microscopy techniques are well suited for imaging fast moving single molecules in two dimensions even within cells. However, the 3D imaging of single molecules poses several technical challenges. Foremost being that in the current microscope design only one focal plane can be imaged at any given point in time. Hence single molecule tracking in a 3D environment such as a cell is problematic since the molecule can easily move out of the focal plane that is currently being imaged. Focusing devices such as piezo nano-positioners could be used to overcome this shortcoming by sequentially scanning the sample at different planes. However, these devices are typically slow and therefore may not be suitable for 3D tracking of fast moving single molecules. Aside from this, widefield microscopes suffer from poor depth discrimination capability. Therefore, there exists significant uncertainty in determining the axial location of the single molecule, especially when the molecule is close to the plane of focus. To overcome the above limitations, we have developed a new microscopy technique called multifocal plane microscopy (MUM) that can simultaneously image distinct planes within the specimen. In contrast to standard microscopes, a MUM setup exhibits significantly improved depth discrimination capability, especially close to focus, which markedly improves the accuracy with which the axial position of the single molecule can be determined. **Results are presented to illustrate the applicability of MUM for 3D single molecule tracking.**

Keywords: Multifocal plane microscopy, 3D single molecule tracking, localization accuracy, Fisher information matrix, maximum likelihood estimation

1. INTRODUCTION

The study of intracellular trafficking events is of fundamental importance to understanding cellular function.^{1,2} The movement of macromolecules to diverse sites in a cell is coordinated by complex transport pathways. For example, endocytic events originate from the plasma membrane, where cargo molecules bound to their cell-surface receptors are taken up through specific mechanisms (e.g., clathrin coated pits) and are transported to endosomal compartments deep inside the cell. Imaging techniques such as total internal reflection fluorescence microscopy³ (TIRFM) and epi-fluorescence microscopy have led to major insights into the nature of trafficking events. The advent of single molecule microscopy has generated significant interest in intracellular trafficking pathways at the individual molecule level.⁴⁻⁶ Single molecule experiments overcome averaging effects and provide information that cannot be obtained with conventional bulk studies.⁷ Such details become crucially important when the system under study is heterogeneous, for example when studying the trafficking pathways of internalized cargo molecules from the plasma membrane to the sorting endosome.

While research efforts have mainly focused on understanding trafficking events occurring either on the plasma membrane or at the cell interior, the 3D trafficking itineraries that span from the plasma membrane to the intracellular compartments have not been well studied. This is largely due to limitations of current widefield imaging techniques. Foremost being that these techniques can image only one focal plane at any given point in

Send correspondence to R.J.O.; E-mail: ober@utdallas.edu

time. Hence the intracellular object (e.g., single molecule, vesicle or tubule) being tracked can easily move out of the focal plane being imaged making it problematic to follow rapid intracellular dynamics in 3D. For instance, in a study that imaged endocytic events on the plasma membrane, the internalizing vesicles could not be tracked deep inside the cell as they moved out of the focal plane being imaged.⁸ Thus the inability to track vesicles in 3D results in a partial reconstruction of the trafficking itinerary, which leaves open many biologically relevant questions, such as the final destination of these vesicles, etc. Additional problems arise when the object to be tracked are single molecules, which typically move very fast even within a cellular environment. In single molecule tracking the accuracy with which their location can be determined plays a crucial role in the interpretation of the results.^{9,10} One of the major shortcomings of widefield microscopes is that they suffer from poor depth discrimination capability.^{11,12} As a result, it is difficult to determine whether a single molecule is in focus or out of focus, especially when the molecule is close to the focal plane being imaged. This in turn introduces a high level of error in determining the axial (z) location of the single molecule. Thus single molecular tracking within a 3D environment such as cell becomes problematic. Aside from this, conventional fluorescent markers that are typically used to label single molecules are not bright and are susceptible to rapid photobleaching thereby placing severe constraints on the detection setup and the duration of imaging. While this can be overcome by using quantum dot (QD) labels, which are extremely bright and photostable, the problem concerning the poor depth discrimination capability of widefield microscopes still remains unsolved.

We have developed an imaging modality called multifocal plane microscopy (MUM) for 3D localization and tracking of sub-cellular objects within a live cell environment.^{6,13,14} In MUM, the sample is simultaneously imaged at distinct focal planes by placing multiple detectors at specific, calibrated distances in the microscope's emission-light path. **This enables us to continuously track intracellular objects within a 3D environment such as a cell. Aside from this, the simultaneous imaging of several focal planes provides superior information about the z-location of the object being tracked thereby overcoming the poor depth discrimination of standard microscopes. Here we present an analysis of the improved depth discrimination capability of MUM and discuss its applicability for 3D single molecule tracking.**

2. RESULTS

2.1 Multifocal plane microscopy

MUM enables simultaneous imaging of multiple focal planes within a cellular specimen. Here we provide a brief description and additional details can be found in Refs. 6,13,14. Fig. 1 shows the schematic of a MUM setup that can simultaneously image three distinct focal planes within the specimen. The specimen is illuminated in widefield mode and the light collected from the sample is split into several paths, each of which has a detector that is placed at a specific, calibrated distance for the tube lens. The sample can be illuminated through total internal reflection fluorescence mode and/or through epifluorescence mode. Our current implementation of MUM supports simultaneous imaging of up to four distinct planes.

2.2 Depth discrimination

The depth discrimination capability is characterized by how accurately the z-location of a microscopic object be determined from its image. To quantify this property for a MUM setup, we adopt a stochastic framework and model the acquired data as a spatio-temporal random process.¹⁰ The task of determining the 3D location of a single molecule from MUM data is a parameter estimation problem. According to the Cramer-Rao inequality,¹⁵ the (co)variance (matrix) of any unbiased estimator $\hat{\theta}$ of θ is always greater or equal to the inverse Fisher information matrix, i.e.,

$$\text{Cov}(\hat{\theta}) \geq \mathbf{I}^{-1}(\theta). \quad (1)$$

The Fisher information matrix provides a quantitative measure of the total information contained in the acquired data about the parameter that we wish to estimate and is independent of how θ is estimated. Because the accuracy of parameter estimates is typically specified in terms of its standard deviation, the above inequality implies that the square root of the (corresponding leading diagonal entry of the) inverse Fisher information matrix provides a lower bound to the accuracy of the estimates of θ . **In the present context, if θ denotes the 3D location of the single molecule then the square root of the leading diagonal entry of the inverse Fisher information matrix corresponding to z_0 provides a limit to the localization accuracy of z_0 .**

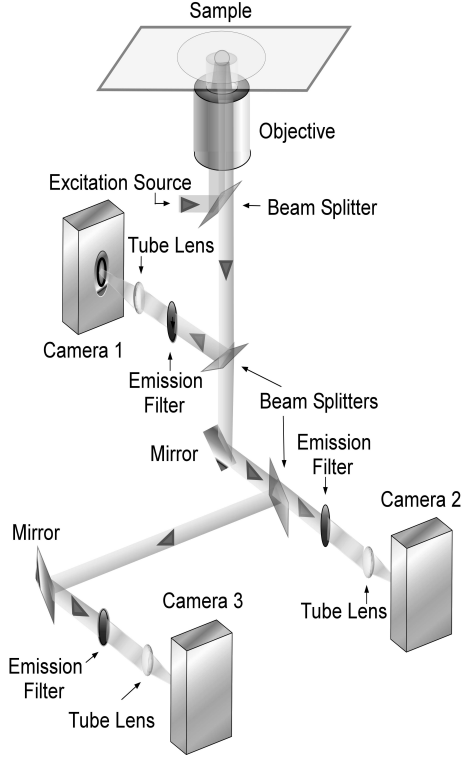


Figure 1. Multifocal plane microscopy. The figure shows the schematic of a multifocal plane microscope that can simultaneously image three distinct planes within the sample. The sample is illuminated in widefield mode and the collected light is split into three paths. In each path, a detector is placed at a specific calibrated distance from the tube lens. This enables the detector to image a distinct focal plane inside the specimen.

2.3 Fisher information matrix

Eq. 1 is a general result. To obtain concrete numbers, we calculate the Fisher information matrix for a two plane MUM setup. In a MUM setup, the data acquired from each focal plane can be assumed to be statistically independent. Hence the Fisher information matrix for the 3D location estimation problem can be written as

$$\mathbf{I}_{tot}(\theta) := \mathbf{I}_1(\theta) + \mathbf{I}_2(\theta) + \dots + \mathbf{I}_N(\theta), \quad (2)$$

where $\theta = (x_0, y_0, z_0) \in \Theta$ denotes the 3D location of the object and $\mathbf{I}_j(\theta)$ denotes the Fisher information matrix corresponding to the j^{th} focal plane image, $j = 1, \dots, N$. The analytical expression for \mathbf{I}_j , $j = 1, \dots, N$ is given by¹⁰

$$\mathbf{I}_j(\theta) := \text{diag} \left[\int_0^t \iint_{\mathbb{R}^2} \frac{\Lambda(\tau)}{q_{z'_0}(x, y)} \left(\frac{\partial q_{z'_0}(x, y)}{\partial x} \right)^2 dx dy d\tau, \int_0^t \iint_{\mathbb{R}^2} \frac{\Lambda(\tau)}{q_{z'_0}(x, y)} \left(\frac{\partial q_{z'_0}(x, y)}{\partial y} \right)^2 dx dy d\tau, \int_0^t \iint_{\mathbb{R}^2} \frac{\Lambda(\tau)}{q_{z'_0}(x, y)} \left(\frac{\partial q_{z'_0}(x, y)}{\partial z_0} \right)^2 dx dy d\tau \right], \quad (3)$$

where $\theta \in \Theta$, t denotes the exposure time, Λ and q denote the photon detection rate and the image function of the object, respectively, $z'_0 := z_0 - \delta_j$ and δ_j denotes the focal plane distance of the j^{th} focal plane in the specimen for $j = 1, \dots, N$. An image function q_{z_0} describes the image of an object at unit magnification that is located at $(0, 0, z_0)$ in the object space.¹⁰ The derivation of the above expression assumes that the photon detection rate Λ is independent of the 3D location, the image function q_{z_0} is laterally symmetric for every $z_0 \in \mathbb{R}$, i.e., $q_{z_0}(x, y) = q_{z_0}(-x, y) = q_{z_0}(x, -y)$, $(x, y) \in \mathbb{R}^2$, $z_0 \in \mathbb{R}$, and the partial derivative of q_{z_0} with respect to z_0

is laterally symmetric, i.e., $\partial q_{z_0}(x, y)/\partial z_0 = \partial q_{z_0}(-x, y)/\partial z_0 = \partial q_{z_0}(x, -y)/\partial z_0$, $(x, y) \in \mathbb{R}^2$, $z_0 \in \mathbb{R}$. It should be pointed out that the above assumptions are typically satisfied for several 3D point spread function models.¹⁶

To compute eq. 3, we require explicit analytical expressions for the image function and its partial derivatives, which are given below.

$$q_{z_0}(x, y) = \frac{1}{C_{z_0}} (U_{z_0}^2(x, y) + V_{z_0}^2(x, y)), \quad (x, y) \in \mathbb{R}^2, \quad z_0 \in \mathbb{R}, \quad (4)$$

where

$$\begin{aligned} U_{z_0}(x, y) &:= \int_0^1 J_0 \left(\frac{2\pi n_a}{\lambda} (\sqrt{x^2 + y^2}) \rho \right) \cos(W_{z_0}(\rho)) \rho d\rho, \quad (x, y) \in \mathbb{R}^2, \quad z_0 \in \mathbb{R}, \\ V_{z_0}(x, y) &:= \int_0^1 J_0 \left(\frac{2\pi n_a}{\lambda} (\sqrt{x^2 + y^2}) \rho \right) \sin(W_{z_0}(\rho)) \rho d\rho, \quad (x, y) \in \mathbb{R}^2, \quad z_0 \in \mathbb{R}, \\ C_{z_0} &= \int_{\mathbb{R}^2} (U_{z_0}^2(x, y) + V_{z_0}^2(x, y)) dx dy, \quad z_0 \in \mathbb{R}, \end{aligned} \quad (5)$$

$(x, y) \in \mathbb{R}^2$ denotes an arbitrary point on the detector plane, λ denotes the wavelength of the detected photons, n_a denotes the numerical aperture of the objective lens, J_0 denotes the zeroth order Bessel function of the first kind and $W_{z_0}(\rho)$, $\rho \in [0, 1]$, denotes the phase aberration term. The term C_{z_0} is the normalization constant, and the $1/C_{z_0}$ scaling in eq. 4 ensures that

$$\frac{1}{M^2} \int_{\mathbb{R}^2} q_{z_0} \left(\frac{x}{M} - x_0, \frac{y}{M} - y_0 \right) dx dy = 1, \quad (x_0, y_0, z_0) \in \Theta,$$

where M denotes the lateral magnification of the objective lens. The phase aberration term W_{z_0} is set to be

$$W_{z_0}(\rho) := \frac{\pi(n_a)^2 z_0}{n_{oil} \lambda} \rho^2, \quad \rho \in [0, 1], \quad z_0 \in \mathbb{R}, \quad (6)$$

where n_{oil} denotes the refractive index of the immersion oil. The partial derivatives of q_{z_0} with respect to x , y , and z_0 are given by

$$\begin{aligned} \frac{\partial q_{z_0}(x, y)}{\partial \zeta} &= \frac{2}{C_{z_0}} \left(U_{z_0}(x, y) \frac{\partial U_{z_0}(x, y)}{\partial \zeta} + V_{z_0}(x, y) \frac{\partial V_{z_0}(x, y)}{\partial \zeta} \right), \quad (x, y) \in \mathbb{R}^2, \quad z_0 \in \mathbb{R}, \quad \zeta \in \{x, y\}, \\ \frac{\partial q_{z_0}(x, y)}{\partial z_0} &= - \frac{U_{z_0}^2(x, y) + V_{z_0}^2(x, y)}{C_{z_0}^2} \frac{\partial C_{z_0}}{\partial z_0} \\ &+ \frac{2}{C_{z_0}} \left(U_{z_0}(x, y) \frac{\partial U_{z_0}(x, y)}{\partial z_0} + V_{z_0}(x, y) \frac{\partial V_{z_0}(x, y)}{\partial z_0} \right), \quad (x, y) \in \mathbb{R}^2, \quad z_0 \in \mathbb{R}, \end{aligned}$$

where for $\zeta \in \{x, y\}$,

$$\begin{aligned} \frac{\partial U_{z_0}(x, y)}{\partial \zeta} &= - \frac{2\pi n_a \zeta}{\lambda \sqrt{x^2 + y^2}} \int_0^1 J_1 \left(\frac{2\pi n_a}{\lambda} (\sqrt{x^2 + y^2}) \rho \right) \cos(W_{z_0}(\rho)) \rho^2 d\rho, \quad (x, y) \in \mathbb{R}^2, \quad z_0 \in \mathbb{R}, \\ \frac{\partial V_{z_0}(x, y)}{\partial \zeta} &= - \frac{2\pi n_a \zeta}{\lambda \sqrt{x^2 + y^2}} \int_0^1 J_1 \left(\frac{2\pi n_a}{\lambda} (\sqrt{x^2 + y^2}) \rho \right) \sin(W_{z_0}(\rho)) \rho^2 d\rho, \quad (x, y) \in \mathbb{R}^2, \quad z_0 \in \mathbb{R}, \\ \frac{\partial U_{z_0}(x, y)}{\partial z_0} &= - \int_0^1 J_0 \left(\frac{2\pi n_a}{\lambda} (\sqrt{x^2 + y^2}) \rho \right) \sin(W_{z_0}(\rho)) \frac{\partial W_{z_0}(\rho)}{\partial z_0} \rho d\rho, \quad (x, y) \in \mathbb{R}^2, \quad z_0 \in \mathbb{R}, \\ \frac{\partial V_{z_0}(x, y)}{\partial z_0} &= \int_0^1 J_0 \left(\frac{2\pi n_a}{\lambda} (\sqrt{x^2 + y^2}) \rho \right) \cos(W_{z_0}(\rho)) \frac{\partial W_{z_0}(\rho)}{\partial z_0} \rho d\rho, \quad (x, y) \in \mathbb{R}^2, \quad z_0 \in \mathbb{R}. \end{aligned}$$

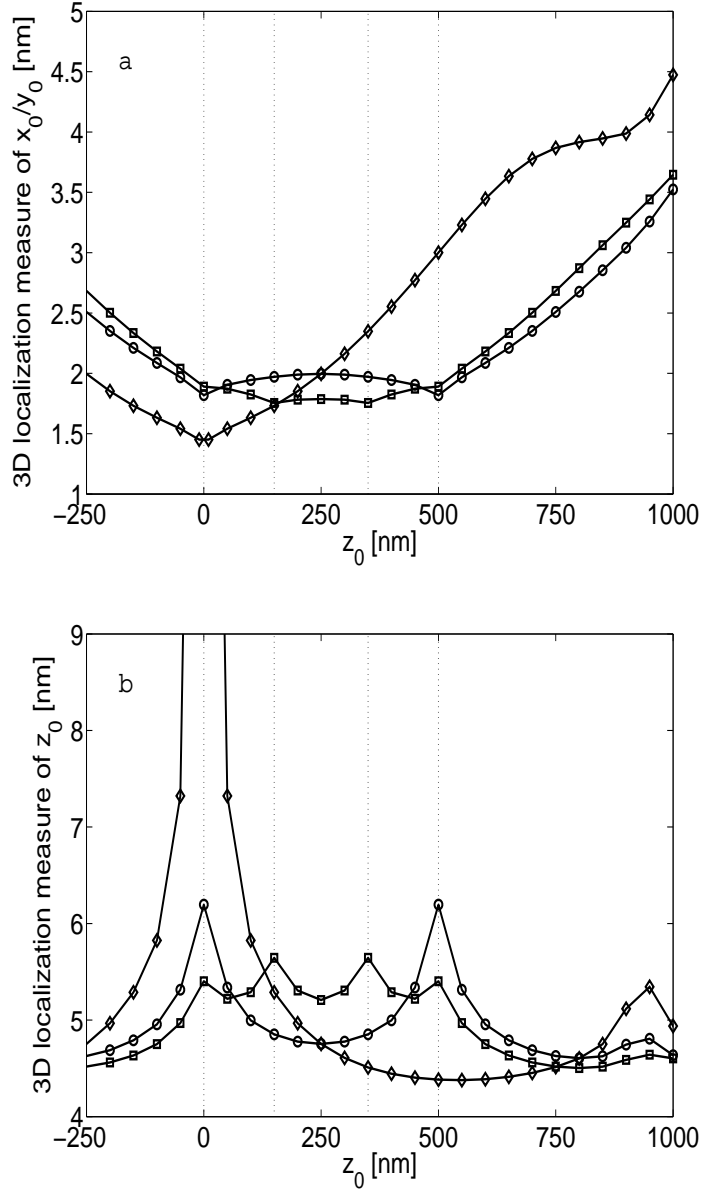


Figure 2. Behavior of the limit of the localization accuracy of x_0 (y_0) and z_0 . Panel A shows the limit of the localization accuracy of x_0 (y_0) as a function of the z -location of the single molecule for a standard microscope (diamonds), for a two plane MUM setup (circles) and for a four plane MUM setup (squares). Panel B shows the same for the z_0 coordinate. **For the standard microscope, the z -location of the single molecule is specified with respect to the focal plane of the objective lens.** For the MUM setup, one of the focal planes is chosen as the reference, **and the z -location of the single molecule and the focal plane distances are specified with respect to the reference plane.** **For the two plane MUM setup, plane 2 is assumed to be at a distance of 500 nm from the reference plane.** **For the four plane MUM setup, planes 2, 3 and 4 are assumed to be at a distance of 150 nm, 350 nm and 500 nm, respectively, from the reference plane.** In both panels, the position of the focal planes are indicated by dotted lines with the reference plane shown at $z_0 = 0$. For all the plots, the numerical aperture of the objective lens is set to $n_a = 1.4$, the wavelength of the detected photons is set to $\lambda = 0.51 \mu\text{m}$, the refractive index of the immersion oil is set to $n_{oil} = 1.515$, the photon detection rate is set to 2000 photons/s ($\frac{2000}{N}$ photons/s/plane) for the standard microscope (N-plane MUM setup) and the exposure time is set to $t = 1$ s.

2.4 Depth discrimination calculations

Figure 2 shows the limit of the localization accuracy of x_0 (y_0) and z_0 as a function of the z-location for a standard microscope, for a two-plane MUM setup and for a four plane MUM setup. Consistent with our previous results,¹¹ we see that for a standard microscope the limit of the localization accuracy of x_0 has the smallest numerical value when $z_0 = 0$ and deteriorates (i.e., becomes large) as the z-location of the single molecule increases (decreases) from $z_0 = 0$ (see 2A). The limit of the localization accuracy of z_0 , on the other hand, is worst when the z-location value of the single molecule is close to $z_0 = 0$ (see Fig. 2B). An immediate implication of this result is that there exist high uncertainty in determining the z-location of a single molecule when it is close to the plane of focus. Hence 3D tracking of single molecules is problematic with a standard microscope.

In contrast to a standard microscope, the limit of the localization accuracy of z_0 for a MUM setup does not deteriorate significantly when the z-value is close to $z_0 = 0$ (Fig. 2B). In particular the limit of the localization accuracy for z_0 remains constant for a range of z_0 values. This implies that with a MUM setup, the z-location of the single molecule can be determined with relatively the same level of accuracy for a range of z_0 values thereby making 3D tracking of single molecules feasible. We have also calculated the limit of the localization accuracy of x_0 for the MUM setup (see Fig. 2A), which also remains constant for a range of z_0 values.

We next investigated how the number of focal planes affects the limit of the localization accuracy for a MUM setup. For this purpose we calculated the results for a two-plane MUM setup and for a four plane MUM setup which are shown in Fig. 2. For the two-plane MUM setup, the distance between the two focal planes in the object space was set to 500 nm. For the four-plane MUM setup, one of the focal planes was set as the reference and with respect to this plane the focal plane spacings of the other three planes were set to 150 nm, 350 nm and 500 nm. **For the x_0 coordinate, we see that the limit of the localization accuracy for the four plane MUM setup is consistently smaller than that for the two plane MUM setup for z_0 values in the range of 50 nm to 450 nm. This implies that the x-location of the single molecule can be more accurately determined with a four plane MUM setup than with a two plane MUM setup when the z-location of the single molecule is in the range of 50 nm to 450 nm.** For all other values of z_0 shown in Figure 2A the limit of the localization accuracy for the four plane MUM setup is greater than that for the two plane MUM setup. **This implies that for these values of z_0 , the x-location of the single molecule can be determined more accurately with a two plane MUM setup than with a four plane MUM setup.** For the z_0 coordinate, we see that the limit of the localization accuracy for the two plane MUM setup is consistently smaller than that for the four plane MUM setup for z_0 values in the range of 100 nm to 400 nm. For all other values of z_0 shown in Figure 2B the limit of the localization accuracy for the two plane MUM setup is greater than that for the four plane MUM setup.

Acknowledgments

This research was supported in part by grants from the National Institutes of Health (R01 GM071048).

REFERENCES

1. I. Mellman, "Endocytosis and molecular sorting.," *Annual Reviews on Cellular and Developmental Biology* **12**, pp. 575–625, 1996.
2. F. R. Maxfield and T. E. McGraw, "Endocytic recycling," *Nature Reviews in Molecular Cell Biology* **5**, pp. 121–132, 2004.
3. D. Axelrod, "Total internal reflection fluorescence microscopy in cell biology.," *Traffic* **2**, pp. 764–74, 2001.
4. S. Y. Kim, Z. Gitai, A. Kinkhabwala, L. Shapiro, and W. E. Moerner, "Single molecules of the bacterial actin MreB undergo directed treadmilling motion in *Caulobacter crescentus*," *Proceedings of the National Academy of Sciences USA* **103**, pp. 10929–34, 2006.
5. R. J. Ober, C. Martinez, X. Lai, J. Zhou, and E. S. Ward, "Exocytosis of IgG as mediated by the receptor, FcRn: An analysis at the single molecule level," *Proceedings of the National Academy of Sciences USA* **101**, pp. 11076–11081, 2004.
6. P. Prabhat, Z. Gan, J. Chao, S. Ram, C. Vaccaro, S. Gibbons, R. J. Ober, and E. S. Ward, "Elucidation of intracellular pathways leading to exocytosis of the Fc receptor, FcRn, using multifocal plane microscopy," *Proceedings of the National Academy of Sciences USA* **104**, pp. 5889–5894, 2007.

7. W. E. Moerner and D. P. Fromm, "Methods of single-molecule fluorescence spectroscopy and microscopy," *Review of Scientific Instruments* **74**(8), pp. 3597–3619, 2003.
8. M. Ehrlich, W. Boll, A. V. Oijen, R. Hariharan, K. Chandran, M. L. Nibert, and T. Kirchhausen, "Endocytosis by random initiation and stabilization of clathrin-coated pits.," *Cell* **118**, pp. 591–605, 2004.
9. R. J. Ober, S. Ram, and E. S. Ward, "Localization accuracy in single molecule microscopy," *Biophysical Journal* **86**, pp. 1185–1200, 2004.
10. S. Ram, E. S. Ward, and R. J. Ober, "A stochastic analysis of performance limits for optical microscopes," *Multidimensional Systems and Signal Processing* **17**, pp. 27–58, 2006.
11. S. Ram, E. S. Ward, and R. J. Ober, "How accurately can a single molecule be localized in three dimensions using a fluorescence microscope?," *Proceedings of the SPIE* **5699**, pp. 426–435, 2005.
12. S. Ram, J. Chao, P. Prabhat, E. S. Ward, and R. J. Ober, "A novel approach to determining the three-dimensional location of microscopic objects with applications to 3d particle tracking," *Proceedings of the SPIE* **6443**, pp. D1–D7, 2007.
13. P. Prabhat, S. Ram, E. S. Ward, and R. J. Ober, "Simultaneous imaging of different focal planes in fluorescence microscopy for the study of cellular dynamics in three dimensions," *IEEE Transactions on Nanobioscience* **3**, pp. 237–242, 2004.
14. P. Prabhat, S. Ram, E. S. Ward, and R. J. Ober, "Simultaneous imaging of several focal planes in fluorescence microscopy for the study of cellular dynamics in 3D," *Proceedings of the SPIE* **6090**, pp. 115–121, 2006.
15. C. R. Rao, *Linear statistical inference and its applications.*, Wiley, New York, USA., 1965.
16. S. F. Gibson and F. Lanni, "Diffraction by a circular aperture as a model for three-dimensional optical microscopy," *Journal of the Optical Society of America A* **6**, pp. 1357–1367, 1989.